Elsevier Editorial System(tm) for Journal of Hydrology

Manuscript Draft

Manuscript Number:

Title: Two-Dimensional Simulation of Flow Hydraulics and Bed-Load Transport in a Mountain Gravel-Bed Stream: the Upper Spanish Creek

Article Type: Research Paper

Section/Category:

Keywords: Bed Load, Sediment Transport, Gravel River, Hydrodynamics, Numerical Model

Corresponding Author: Dr. Jennifer Guohong Duan, Ph.D

Corresponding Author's Institution: Desert Research Institute

First Author: Jennifer G. Duan, Ph.D.

Order of Authors: Jennifer G. Duan, Ph.D.; Dong Chen, Ph.D.; Jennifer Weller, MS; Terry Benoit, BS

Manuscript Region of Origin:

Abstract: Abstract
Sediment transport in a gravel-bed mountain stream, the Upper Spanish Creek, California, was simulated with a depth-averaged, two-dimensional hydrodynamic and sediment transport model. The hydrodynamic model is based on the solution of depth-averaged flow continuity and momentum equations with dispersion terms to account for the effect of secondary flow. The sediment transport model treats bed load and bed material as mixtures of multiple grain-size sediment. Changes in bed elevation are calculated by solving the sediment mass conservation equation. A laboratory experiment on sand-bar formation and transverse sediment sorting during an unsteady flow event was selected to verify the sediment-transport model. A comparison of the simulated bar/pool bed configurations and size distribution of surface-bed material with the laboratory measurements indicated the developed model is capable of simulating bed topography and

non-uniform sediment sorting under unsteady flow. The verified model was applied to predict bed-load transport in the Upper Spanish Creek to identify areas of high-erosive potential that require bank protections. Results of this verification process demonstrated the applicability of the two-dimensional hydrodynamic and sediment transport model to assist river restoration designs for gravel-bed streams.

# Two-Dimensional Simulation of Flow Hydraulics and Bed-Load Transport in a Mountain Gravel-Bed Stream: the Upper Spanish Creek

Jennifer G. Duan[1], Dong Chen[1] ,Jen Weller[2,3],Terry Benoit[4]

1. Desert Research Institute, Division of Hydrologic Sciences, 755 E. Flamingo Road, Las Vegas, NV 89119.
2. Desert Research Institute, Division of Hydrologic Sciences, 2215 Raggio Parkway, Reno, NV 89512
3. University of Nevada, Reno, Department of Hydrologic Sciences, Reno, NV 89557
4. Geomorphologist, Plumas Corporation, Quincy, CA 95971.

## Abstract

Sediment transport in a gravel-bed mountain stream, the Upper Spanish Creek, California, was simulated with a depth-averaged, two-dimensional hydrodynamic and sediment transport model. The hydrodynamic model is based on the solution of depth-averaged flow continuity and momentum equations with dispersion terms to account for the effect of secondary flow. The sediment transport model treats bed load and bed material as mixtures of multiple grain-size sediment. Changes in bed elevation are calculated by solving the sediment mass conservation equation. A laboratory experiment on sand-bar formation and transverse sediment sorting during an unsteady flow event was selected to verify the sediment-transport model. A comparison of the simulated bar/pool bed configurations and size distribution of surface-bed material with the laboratory measurements indicated the developed model is capable of simulating bed topography and non-uniform sediment sorting under unsteady flow. The verified model was applied to predict bed-load transport in the Upper Spanish Creek to identify areas of high-erosive

potential that require bank protections. Results of this verification process demonstrated the applicability of the two-dimensional hydrodynamic and sediment transport model to assist river restoration designs for gravel-bed streams.

## Introduction

Restoration of impaired natural channels often requires a multi-dimensional, hydrodynamic and sediment transport model to evaluate restoration scenarios (Duan and Nanda, 2006). Depth-averaged, two-dimensional (2-D) models have been applied to many river restoration projects because a 2-D model requires less computational power and is cost-effective when dealing with practical engineering problems. Among 2-D models presented in the literature, some (Shimizu and Itakura, 1989; Molls and Chaudhry, 1995; Ye and McCorquodale, 1997; Jia and Wang, 1999; Duan et al., 2001; Hsieh and Yang, 2003) have solved the classical, depth-averaged Navier-Stokes equations numerically; others have solved the depth-averaged Navier-Stokes equations (Odgaard 1989a,b; Yen and Ho, 1990; Ye and McCorquadale, 1997; Lien et al., 1999; Duan, 2004; Duan and Julien, 2005) by including the secondary flow correction terms in the momentum equations.

Since secondary flow moves toward the outer bank near the water surface and toward the inner bank near the bed surface, shear force, which moves in the same direction as the local flow close to the bed, deviates slightly from the direction of the mean flow (Engelund and Skovgaard, 1973). Secondary flow correction terms are needed in the momentum and mass transport equations to account for the effects on redistribution of flow momentum and redirecting sediment transport. The empirical relations given by Engelund and Skovgaard (1973) and Shimizu and Itakura (1989) are only valid for

predicting the transverse component of velocity near the bed. The method of Yeh and Kennedy (1993a) is similar to that of Odgaard (1989a) where distribution of the transverse component of velocity is linear and is related to its value at the free surface. Odgaard (1989a) obtained the transverse component of velocity by evaluating the momentum equations at the water surface. Yeh and Kennedy (1993a) obtained the transverse component of velocity by solving the moments of momentum equations. Lien et al. (1999) calculated the dispersion terms in the momentum equations, which are the integrations of the product from the difference between the depth-averaged and actual velocity along the verticals. Odgaard (1989a,b), Crosato (1990), Shimizu and Itakura (1989), and Darby et al. (2002) applied bend-flow models to natural meandering channels. However, these models have not been used to simulate sediment sorting in curved channels. Duan et al. (2001), Duan and Julien (2005), and Duan and Nanda (2006) have applied a 2-D model to simulate sediment transport in laboratory flumes and natural rivers where bed material is quasi-uniform sand.

The objective of this paper is to report the application of an enhanced, 2-D flow hydrodynamic and sediment transport model called the EnSed2D model (Duan, 2004; Duan and Julien, 2005; and Duan and Nanda, 2006) used to predict the rate of bank erosion in the Upper Spanish Creek, California, a gravel-bed mountain stream. The model was first verified through an experimental case of non-uniform sediment sorting in meandering channels. Then, a bed-load transport predictor (Parker, 1990) was calibrated and verified by using bed-load measurements from the Upper Spanish Creek. Bank erosion consists of two processes: basal erosion and bank failure. The rate of bank erosion was calculated based on flow hydraulic forces, sediment transport near banks,

and the probability of bank failure. Reaches that demonstrated high rates of bank erosion were identified based on the calculation. Finally, the modeling results were used to guide the river restoration design.

## Hydrodynamic Model

The governing equations for flow simulation are the depth-averaged Reynolds approximations of the continuity equation (Eq. 1) and momentum equations (Eq. 2).

$$\frac{\partial(hu_j)}{\partial x_j} = 0 \tag{1}$$

$$\frac{\partial(hu_i)}{\partial t} + \frac{\partial(hu_i u_j)}{\partial x_j} + \frac{\partial(hD_{ij})}{\partial x_j} = -gh\frac{\partial \zeta}{\partial x_i} + \frac{\partial}{\partial x_j} h(\nu \frac{\partial u_i}{\partial x_j} - \overline{u_i' u_j'}) - \tau_{bi} \tag{2}$$

$$-\overline{u_i' u_j'} = \nu_t (\frac{\partial u_i}{\partial x_j} + \frac{\partial u_j}{\partial x_i}) - \frac{2}{3} k\delta_{ij} \tag{3}$$

where $u_i$ and $u_j$ are depth-averaged velocity components; $t$ is time; $\zeta$ is surface elevation; $h$ is flow depth; $g$ is acceleration of gravity; $\tau_{bi}$ are friction shear stress terms at the bed surface, written as $\tau_{bi} = \frac{n^2 g}{h^{\frac{1}{3}}} u_i U$, where $U$ is the depth-averaged total velocity and $n$ is Manning's roughness coefficient; $\nu_t$ is eddy viscosity; $\nu$ is kinetic viscosity; and $D_{ij}$ are dispersion terms resulting from the discrepancy between the depth-averaged velocity and actual velocity with their expressions shown as follows:

$$D_{ij} = \int_{z_0}^{z_0+h} (\overline{\overline{u_i}} - u_i)(\overline{\overline{u_j}} - u_j) dz \tag{4}$$

where $z_0$ is the zero velocity level and $\overline{\overline{u_i}}$ and $\overline{\overline{u_j}}$ are depth-averaged velocities. To include the effect of secondary flow, two dispersion terms were added to the momentum

equations. The derivations of these dispersion terms were included in Duan (2004) and Duan and Julien (2005) where the stream-wise velocity satisfies the logarithmic law, and the transverse velocity profile of the secondary flow is assumed to be linear thus satisfying the distribution function of Odgaard (1989a). Details of the hydrodynamic model are provided in Duan (2004), Duan and Julien (2005), and Duan and Nanda (2006).

## Sediment Transport Simulation

The sediment transport model treats bed load and bed material as mixed, grain-size sediment and divides bed load into ten groups. The mean size for each group is denoted by $D_{10}, D_{20}, D_{30}, ..., D_{100}$ where $D_q$ represents the particle size where *q percent* of the sediment is finer. The mean particle size for each group was input as initial conditions. As deposition or erosion occur, mean particle size changes. Traditionally, the rate of sediment transport has been defined as the amount of mono-granular material transported by the stream. Sorting of surface-bed material or selective transport occurs when the bed surface is covered with mixed grain-size sediments. The sediment mixture could be unimodal or bi-modal depending on composition of the bed material. For a sand-gravel mixture, selective transport means that either coarser particles impose a hiding effect on finer particles or different size particles transport at different angles due to the effect of flow-induced shear stress and gravitational forces on a sloping bed. When non-uniform sediment is transporting through curved channels, not only are active deposition and erosion occurring but sorting is also occurring. Because each size fraction is affected by the presence of other fractions, the transport capacity of the *k*th fraction of sediment is related to the transport capacity calculated by using the mean-sized sediment, percentage

of fraction present, and a hiding/exposure factor accounting for the interaction of each size class. A hiding function was used to quantify the influence of larger-sized particles on smaller ones.

## Bed-Load Transport

Numerous equations are available to predict the fractional transport rate of bed-load sediment. To simulate non-uniform sediment transport in curved channels, a non-uniform, bed-load transport formula must be selected. Bed-load transport formulas (Meyer-Peter and Muller, 1948; Yang, 1984, etc.) originally were not intended for application to individual-sized classes of a mixture. Therefore, a hiding factor, such as Einstein (1950), was used to allocate the total transport rate calculated by using the median diameter of each individual-sized class. The hiding factor is an exponential function of the ratio between the mean particle size of each individual-sized class and the mixture employed in Einstein (1950), Rahuel et al. (1989), Armanini and Di Silvio (1988), and Wu et al. (2001). To simplify the procedure, shear stress based on the Meyer-Peter bed-load equation was employed for the experimental case (Yen and Lee, 1995) in the present study. In the case of the Upper Spanish Creek, a bed-load transport equation was chosen and calibrated based on field measurements of bed-load transport. A hiding function (Parker et al., 1982, Parker 1990) was adopted as a calibration factor to allocate the bed-load transport rate for the individual size fraction and is written as follows:

$$\eta_i = \left(\frac{D_i}{D_{50}}\right)^{\chi} \tag{5}$$

where $\chi$ is an exponent. If $\chi = 0$, the bed-load transport rate for each size fraction is independent of particle size; $\chi = 1$, the bed load transport is size selective and proportional

to particle size. Additionally, secondary flow results in bed-load transport and deviates from the direction of mean flow velocity in meandering channel. The angle of deviation ϕ can be expressed as follows:

$$\tan\phi = \frac{q_n}{q_s} = \frac{u_{bn}}{u_{bs}} - \beta\frac{\partial\eta}{\partial n} \tag{6}$$

where $\beta = \beta^*\left(\frac{\tau_c^*}{\tau^*}\right)^m$ and $s$ and $n$ are the downstream and transverse directions; $q_s$ and $q_n$ are the volume sediment transport rates per unit width per unit time in the $s$ and $n$ directions; $u_{bs}$ and $u_{bn}$ are the corresponding near-bed flow velocities; the parameter $\tau$* is the Shields parameter related to the downstream bed- shear stress $\tau_s$ by the relation $\tau^* = \tau_s/(\rho(G-1)gd)$ in which $G$ is the specific gravity of the sediment; $g$ is the gravitational acceleration; $d$ is the grain diameter; $\tau_c^*$ is the critical value of $\tau$* at the threshold of motion; and $\eta$ is the bed elevation, such that $-\partial\eta/\partial n$ is the transverse bed slope. Different values for coefficient $\beta^*$ and exponent $m$ are available in the literature (Hasegawa, 1981). The present study adopted the relation of Engelund and Fredsoe (1982) where $\beta^*$ equals 1/1.6.

The first term on the right side of Eq. 6 accounts for the effect of secondary flow velocity at the bed surface, and the second term quantifies the effect of transverse slope. Therefore, the direction of bed-load transport in Cartesian coordinates, denoted by $x$ and $y$, can be obtained as follows:

$$\begin{bmatrix} a_x \\ a_y \end{bmatrix} = \begin{bmatrix} \cos\theta & -\sin\theta \\ \sin\theta & \cos\theta \end{bmatrix}\begin{bmatrix} \cos\phi \\ \tan\phi\cos\phi \end{bmatrix} \tag{7}$$

where $\theta$ is the angle between the centerline and positive x axis; $\phi$ is the deviation angle; and $\alpha_x$ and $\alpha_y$ denote the fractional components of bed-load transport in the $x$ and $y$ directions, respectively.

## Bed-Elevation Changes

To simulate degradation or aggradation, bed-load transport rate is needed in the mass conservation equation. The bed-load transport equation within the mixing layer for each individual size class is solved as follows to calculate the bed-elevation change:

$$(1-\lambda_p)\frac{\partial Y_k}{\partial t}+\frac{\partial \alpha_x q_{bk}}{\partial x}+\frac{\partial \alpha_y q_{bk}}{\partial y}=0 \tag{8}$$

where $\lambda_p$ is the porosity of bed material; $Y_k$ is the bed elevation associated with the $k$th group sediment; and $q_{bk}$ is volumetric bed load transport rate for $k$th size group. Eq. 8 indicates that the change in bed elevation depends not only on the gradient of the bed-load transport rate but also on the direction of bed load transport.

## Boundary Conditions

At the inlet, the total discharge is a constant for steady flow simulation. The total discharge is distributed along the cross section according to the local conveyance as follows:

$$q_i = K\frac{h_i^{\frac{5}{3}}}{n} \tag{9}$$

where $q_i$ is unit discharge; $K$ is the local conveyance coefficient; and $n$ is Manning's roughness coefficient. The current version of the model allows the specifications for the roughness coefficient to be denoted as roughness height or Manning's roughness

coefficient for each computational node. However, for the experimental cases described in this paper, the roughness coefficient was a constant based on the bed roughness conditions described in the original experiments. Because total discharge can be calculated as the integral of unit discharge across channel width, the following equation applies:

$$Q = \int q_i ds = K \int \frac{h_i^{\frac{5}{3}}}{n} ds \tag{10}$$

where $s$ denotes the direction of channel width and $K$ is the flow conveyance. At the outlet, surface elevation is set as a constant to reflect the observed surface elevation. The velocity at the outlet cross section is calculated based on total discharge and flow depth. At the sidewall, the logarithmic law is applied to the wall boundary. After the gradient of velocity is determined, the velocity at the sidewall is calculated based on the velocity at the adjacent internal node.

Sediment boundary conditions including bed-load sediment at the inlet are determined based on the individual experimental case. At the side walls, the sediment transport rate is assumed to be equal to the transport rate at adjacent internal nodes. At the outlet section, the sediment transport rate equals the transport rate at the immediate upstream cross section, and bed elevation at the outlet cross section is kept unchanged through the computation.

## Test and Verification

### Case 1: Non-Uniform Sediment Sorting in a Curved Channel

Yen and Lee (1995) conducted experiments in a laboratory channel bend having a central angle of 180°. Channel width was 1 m, and the radius of the centerline curvature was 4 m. The bend was connected to a stilling basin with an upstream straight reach of 11.5 m and a downstream straight reach of the same length. A 20-cm-thick layer of sand with 8 different particle size groups with $d_0$ equaling 1.0 mm and $\sigma_o$, (size deviation) equaling 2.5 was placed on the bed before each experimental run. Hydrographs with base flows of 0.02 $m^3/s$ and maximum peak flows of 0.075 $m^3/s$ were released at the upstream. The base flow provided the critical flow condition to entrain sediment having a mean size of 1.0 mm. Five experimental runs were conducted with five different peak flow discharges. Measurements of bed elevations were taken with a point gauge at the peak and end of the hydrograph for each experiment after flow was stopped and water was completely but slowly drained. Samples of the surface-bed layer were taken at six locations, and these samples were dried, weighed, and sieved for size gradation. This series of experiments demonstrated that maximum transverse slopes were formed at the experimental flume and sorting of non-uniform sediments increased with unsteadiness in the flow hydrograph.

In the present study, we simulated experimental run #3, with flow parameters (e.g., discharge, peak duration) summarized in Table 1. The base flow discharge was 0.02 $m^3/s$, which is equivalent to the condition for incipient motion of the median particle size. The peak flow discharge ranges from 0.0613 to 0.075 $m^3/s\, m^3/s$. Experimental results for bed topography and sediment-size gradation (Yen and Lee, 1995) are shown in Fig. 1.

The hydrodynamic model and sediment transport model were decoupled for the simulations. The hydrodynamic flow field initially was obtained by simulating the base

flow condition with a constant discharge of 0.02 $m^3/s$. Then flow hydrographs were input as the upstream boundary conditions, and the flow field was recalculated for each discharge. The sediment transport rate and sediment continuity equation were solved based on the solved flow hydrodynamic field. The time step for flow calculations is different from the time step for sediment calculations. The time step for sediment calculations is limited by criteria for the maximum change in bed elevation at each time step, which should be less than 0.2 percent of the flow depth, and the maximum sediment time step, which must be less than 60 s.

During the simulation, the hiding function was employed as a calibration factor by varying the exponent $\chi$ from 0 to 1.0. The closest matches with experimental measurements result when $\chi$ equals 0.56. The transport of bed bed-load mixture becomes more selective as the value of $\chi$ increases. The simulated bed topography and mean sediment size for this run are plotted in Fig. 2. Results showed the formation of sand bars and the size distribution of surface bed material where sand bar surfaces have finer particles and pool areas consist of coarser particles. In addition, these results demonstrated the effects of the hiding factor in modeling selective sediment transport in curved channels. Since there is no analytical expression for the hiding factor, it was used as a calibration parameter depending on sediment-size distribution.

## Case 2: Bed-Load Transport Simulation in the Upper Spanish Creek

### *Bed-load Transport Equation for the Study Reach*

Selection of an appropriate bed-load transport equation is an important consideration in numerical modeling of sediment transport. Numerous equations have been developed to predict bed-load transport in gravel-bed streams; however, because the mechanics of

sediment transport are not fully understood, bed-load transport equations can be an additional source of uncertainty. In this section we discuss available methods for selecting appropriate sediment-transport equations and calibrating equations with field data from the Upper Spanish Creek.

The Upper Spanish Creek is a heavily armored gravel-bed stream; therefore, only surface-based fractional transport models were considered (Parker, 1990; Wu et al., 2000; and Wilcock and Crowe, 2003). The total material transported during a storm depends on flow intensity, flood duration, proximity of flood to other events, and sediment supply. Because the selected bed-load equations are based solely on hydraulic properties and surface-material characteristics, the phenomena of bed loosening and/or armoring have not been considered adequately in the predicted results for bed-load transport.

There are several noticeable differences among the sediment equations used in this study. The Parker (1990) equation is based on field data; however; bed-load is truncated at 2 mm. The Wilcock and Crowe (2003) equation, based on experimental flume datasets, accounts for the entire grain-size distribution and allows sand and gravel to move at separate rates. Both the Parker (1990) and Wilcock and Crowe (2003) equations scale the fractional transport rate by the same dimensionless parameter, $\frac{(\rho_s / \rho - 1)g}{u_*^3 p_i}$, which is based on the percentage of the *i*th-size-class sediment, $p_i$, in the surface material. Wu et al. (2000) based their equation on both field and experimental datasets and scaled their fractional transport rate with the following expression: $p_i \sqrt{(\gamma_s / \gamma - 1) g d_i^3}$. However, they did not include shear velocity, $u_*$. The Wu et al. (2000) equation uses independent variables in the ordinate and abscissa parameters, while the Parker (1990) and Wilcock

and Crowe (2003) equations use dependent variables in both coordinates.

All three equations include a function to represent hiding and exposure of different size particles relative to the overall size distribution in the surface sediment, expressed as the exponential of the ratio between the individual-size class and the mean-size class. The Wu et al. (2000) equation derived the hiding function as a ratio between the probability of hiding and the probability of exposure.

For the present study, the Parker (1990) bed-load transport model provided the best match to the field data collected during the snowmelt season in spring 2005. Parker's (1990) surface-based equation is an extension of the substrate-based model of Oak Creek, Oregon, described in Parker et al. (1982). Since this model was developed specifically for Oak Creek, its applicability to other rivers is limited by the constant parameters determined from the Oak Creek data set. The mathematical expression for the Parker (1990) equation follows:

$$W = \sum W_i F_i = 0.00218 \sum G(\phi) F_i \text{ and } \phi = \omega \phi_{sg0} g_0(\delta_i) \tag{11}$$

where $W$ is the total transport rate and $W_i$ is the dimensionless bed-load transport rate for the *i*th-size fraction defined as follows:

$$W_i = \frac{(S-1) g q_{bi}}{u_*^3 F_i} \tag{12}$$

where $S$ is the ratio of sediment density to water density; $g$ is acceleration due to gravity; $q_{bi}$ is the total bed-load transport rate per unit width of the *i*th-size fraction; $u_*$ is the shear velocity defined as $u_* = \sqrt{\tau / \rho}$; and $F_i$ is the portion of *i*th-size sediment in surface-bed material calculated after sand is removed. The function $G(\phi)$ is the fractional bed-load

transport equation expressed as follows:

$$G(\phi) = \begin{cases} 5474\left(1 - \dfrac{0.853}{\phi}\right)^{4.5} & \phi > 1.59 \\ \exp\left[14.2(\phi - 1) - 9.28(\phi - 1)^2\right] & 1 \le \phi \le 1.59 \\ \phi^{M_0} & \phi \le 1 \end{cases} \tag{13}$$

where the constant $M_0$ equals 14.2 and

$$\phi = \omega \phi_{sg0} g_0(\delta_i) \text{ and } \phi_{sg0} = \frac{\tau^*_{sg}}{\tau^*_{rsg0}}, \tau^*_{sg} = \frac{\tau}{\rho R g D_{sg}} \tag{14}$$

where $\tau^*_{sg}$ is Shields stress based on the geometric mean size in surface material; $\phi_{sg0}$ is the dimensionless Shields stress; $D_i$ is the geometric mean-grain size of the *i*th-size fraction; $D_{sg}$ is the geometric mean-grain size of the surface material with sand included. The constant, $\tau^*_{rsg0}$ = 0.0386, is specifically determined from the Oak Creek field data. The parameter $\omega$ is defined as follows:

$$\omega = 1 + \frac{\sigma_\phi}{\sigma_{\phi 0}}(\omega_0 - 1) \tag{15}$$

where

$$\sigma^2_\phi = \sum\left[\frac{\ln(D_i / D_{sg})}{\ln(2)}\right] \tag{16}$$

and $\omega_0$ and $\sigma_{\phi 0}$ are straining functions of $\phi_{sg0}$, which can be found in Fig. 5 of Parker (1990). The parameter $g_0(\delta_i)$ denotes a surface-based hiding function given as follows:

$$g_0(\delta_i) = (\delta_i)^{-\beta} \tag{17}$$

where $\beta = 0.0951$, $\delta_i = D_i / D_{sg}$, and $\ln D_{sg} = \sum F_i \ln D_i$.

The Parker model is unique because it is based solely on field observations of bed-load transport. Although this equation was formulated for the Oak Creek, Oregon, model, which utilizes one of the most comprehensive field datasets for bed-load transport (Milhous, 1973), empirical coefficients must be calibrated for applications to other rivers. Uncertainty may arise when the Parker (1990) equation is applied to a model that addresses mixed sand and gravel sediments, since the Parker (1990) equation excludes particles finer than 2 mm. Transport equations for sand and gravel mixtures, such as the Wilcock and Crowe (2003) equation, are relatively new and have not been tested widely or applied to natural rivers. In the Upper Spanish Creek, sand content in surface material is less than 10 percent, so the Parker equation should predict adequately most size fractions of bed load. Previous numerical modeling studies have employed successfully the Parker (1990) equation to predict bed-load transport in laboratory experiments and natural rivers (Sutherland et al., 2002; Cui et al., 2003a; Cui et al., 2003b; and Cui and Parker, 2005).

The Parker (1990) bed-load model was calibrated using portable bed-load trap data and then verified with historical Helley-Smith data. Empirical coefficients in Parker (1990) were modified because the original coefficients were determined based solely on field data from the Oak Creek, Oregon, model. The exponent $\beta$ in Eq. 17 was increased from 0.0951 to 0.1500 in order to reflect divergence from the "equal mobility" hypothesis, rendering finer grains more mobile than coarser grains. Bed-load observations indicate that the size distribution of transported material falls between the compositions of both surface and substrate material. Mobility that is truly equal occurs

when bed-load has the same size distribution as substrate (Parker, 1982). The reference Shields stress, $\tau^*_{rsg0}$, was also adjusted from 0.0386 (Eq. 14) to 0.0195, an appropriate value for the geometric mean of the surface-grain size in the Upper Spanish Creek, which was 20.5 mm at the bed-load sampling site. Oak Creek has a coarser surface armoring layer with a mean size of 47 mm, so the reference shear stress is significantly reduced for the Upper Spanish Creek.

The calibrated model produced a root mean square error (RMSE) value of 1.82 when compared with 9 observations of bed-load transport and passed through nearly half of the 6 Helley-Smith data points used in verifying the model. The accuracy of the measured bed-load data used for comparison and calibration is limited by the accuracy in the bed-load samplers used to collect the data. In this study, poor correlation between calculated and measured bed-load is attributed to limitations in the accuracy of field measurements for bed-load transport.

### *Bank-Erosion Calculation*

Bank erosion consists of two processes: basal erosion due to fluvial hydraulic force and bank failure under the influence of gravity. Because the force of bank resistance varies with the degree of saturation in the bank material, the probability of bank failure is the probability of the driving force of bank failure being greater than the bank resistance force. The degree of saturation of bank material increases with river stage; therefore, frequency of bank failure is correlated to frequency of flooding. Consequently, the rate of bank erosion is due both to basal erosion and bank failure, and bank failure is a probabilistic phenomenon. The analytical equation for calculating the rate of bank erosion can be written as presented in (Duan, 2005):

$$M = \frac{\Delta B}{\Delta t} = eE(1 - \frac{\tau_{bc}}{\tau_{b0}})^{\frac{3}{2}} \sqrt{\tau_{b0}} \tag{18}$$

where $e$ is the factor that reflects the effect of bank failure, which incorporates not only bank geometry but also probability of bank failure, and $E$ is the erosion coefficient from the derivation of the basal erosion formula expressed as follows:

$$E = \sin\overline{\beta} \sqrt{\frac{C_L^{'}}{3\rho_s}} \left( 1 - \frac{C}{C_*} \cos\overline{\beta} \right) \tag{19}$$

The erosion coefficient, $E$, relates to the averaged bank angle, coefficient of lift force, and depth-averaged, equilibrium concentration of suspended sediment. The erosion coefficient $e$ in Eq. 18 can be written as follows:

$$e = \frac{\frac{H - Y}{\tan\beta_c} - \frac{H^{'}}{\tan\beta}}{\frac{H - H^{'}}{2\tan\beta} + \frac{\overline{\xi}}{\eta}} \tag{20}$$

where $H$ is the bank height at the critical condition; $H'$ is the bank height above the zone of lateral erosion; $\beta_c$ is the angle of the failure plane; $Y$ is the depth of the tension crack; $\overline{\beta}$ is the averaged bank slope; $\overline{\xi}$ is the depth-averaged bank erosion rate due to hydraulic force; and $\eta$ is the probability of bank failure.

The coefficient of lift force, $C_L'$, in Eq. 19 was calculated by using $C_L = 0.178$. The ratio between the actual and equilibrium concentration of suspended sediment is assumed to be 0.25 based on field observations. The concentration of near-bank suspended sediment can be measured with a suspended sediment sampler. The equilibrium concentration of suspended sediment can be calculated from flow parameters by using the

Van Rijn (1989) formula. The angle of initial bank surface is assumed to be 70° (1.22 in. radian). The basal erosion coefficient calculated from Eq. 19 was calculated for both banks at each cross section.

The actual shear stress was obtained from the hydrodynamic modeling results. Critical shear stress in cohesive bank material is difficult to determine due to complex electrochemical environments. Available formulas for determining critical shear stress in cohesive sediments finer than 0.1 mm are applicable only to irrigation canals and ditches. Cohesion in the bank material resulted from vegetation roots and layers of cohesive silt. Therefore, the approximate critical shear stress was calculated from the Shield's diagram due to lack of an appropriate equation for calculating critical shear stress in cohesive banks.

The critical bank height, *H*, and surface angle of bank failure, $\beta_c$, were calculated by trial and error. The coefficient, *K*, quantifies the depth of the tension crack, which was calculated as the ratio of depth in the tension crack to the critical bank height. The angle of repose used in calculating critical bank height was 35°. Effective cohesion in the bank material was 50 kN/m$^2$, and the density of bank material was 2,650 kg/m$^3$. The initial angle of bank surface was 1.22 in radius. Due to the lack of hydrologic records, probability of bank failure was assumed to be 26 percent based on other related studies of rivers in semi-arid and arid environments.

### *Simulated Results*

To identify sub-reaches prone to bed degradation and bank erosion, the present study simulated a bankfull event. The bankfull event had a return frequency of 2 years, and the

rate of discharge was 130 $m^3/s$ and a duration of 7 days. Fractional bed-load transport rates were calculated by using the Parker (1990) equation with modified coefficients. Bed-elevation change was obtained by solving Eq. 8. Simulated flow depth and velocity were plotted in Fig. 3a and 3b and Fig. 4a and 4b, respectively. The maximum flow depth was approximately 7 m near the concave banks on the upstream reach and at one location on the downstream reach near the town of Quincy. The overall flow depth, denoted with green color, was approximately 3–4 m, and the lower reach was shallower than the upper reach. Flow velocity ranged from 0.16–2.4 m/s with the maximum velocity zone existing near the concave banks. These results indicated that bed-elevation change after a 7-day bankfull event was not significant.

Bed-elevation change was plotted in Fig. 5a and 5b. Deposition dominated in the study reach. After this 7-day bankfull event, there was a 10-cm deposition over the entire study reach. The maximum deposition depth was 50 cm. Bed-surface degradation only occurred in a few locations near the concave banks.

The distance of bank erosion at each cross section was calculated using Eq. 18 and plotted in Fig. 6. The maximum bank-erosion distance was 16 cm after the bankfull event. Sub-reaches where the bank-erosion distance was larger than 10 cm are marked with dark red lines in Fig. 7. The results showed that only several cross sections were eroded at the upstream reach. At the downstream reach, bank erosion occurred at numerous cross sections with an average bank-erosion distance of 5 cm at both banks. Therefore, the downstream reaches will be widened with increased bed elevation after a bankfull event. The highly vulnerable places for bank erosion are marked in Fig. 7. Most banks that experienced a high rate of erosion were located at the concave banks within

the study reach.

In summary, simulated results produced by the EnSed2D model showed overall aggradation in the study reach after a 7-day bankfull flow event. Bed degradation occurred near several concave banks where the rate of bank erosion was high. According to these results, a preliminary restoration design was proposed. The objective of the restoration design was to reduce sediment aggradation at the lower reach and increase stability with bank-protection structures.

The preliminary design includes a detention basin at the upstream with riprap structures emplaced at locations where the banks are prone to erosion. The sediment detention basin will be located between cross section #120 and #200. This basin will utilize the natural topographic setting thus increasing the channel width and lowering the elevation of sand bars and the floodplain. Flow passing through the Devil's Elbow will slow down in the detention basin where gravel sediments are expected to deposit. The exact location and dimensions of the detention basin should be designed following a detailed field survey to determine locations, alignments, and dimensions of bank-protection structures. The detention basin should be inspected and maintained annually at the beginning of the high-flow season to verify that adequate storage capacity is available.

Other engineering measures, including riprap structures and short dikes, should be emplaced to protect banks from erosion. At the upstream reach, one long riprap should be emplaced immediately preceding the detention basin. This riprap structure will protect the concave bank from erosion and stabilize the transition from a naturally flowing river to a man-made detention basin. Two long riprap bank protections structures should be

emplaced in the downstream reach: one at the location where the channel turns to the northeast and the other at near the end of the study reach. Bank materials at both locations consist of fine sediment with silt and fine sands. Short dike structures may be needed with the riprap bank–protection structures to mitigate potential erosion at the banks. At other locations, several short riprap bank-protection structures are proposed. These riprap structures are intended to protect the banks from erosion and prevent the development of meandering bends. If necessary, appropriate bio-engineering approaches should be included in the design of bank-protection structures.

This conceptual design was based on the 2-D EnSed2D modeling results. Detailed geometries for the proposed detention basin and riprap bank-protection structures must be determined according to the flow velocities and shear stresses acting on the banks. Upon approval of the preliminary design, detailed field surveys will be required to determine the locations, alignments, and dimensions of bank-protection structures.

## Conclusions

The computational modeling results of flow hydraulics and sediment transport processes indicated that it is feasible to use a depth-averaged, 2-D model to simulate the hydrodynamic flow field and transport of sediment in mountain gravel-bed streams. There is no doubt that a three-dimensional, hydrodynamic model is needed to simulate the complex flow phenomena such as separation and reverse in mountain streams. However, a depth-averaged, 2-D model has advantages in being cost-effective and easy to calibrate and in requiring less input data for practical engineering applications.

For the planning stage of a project, a 2-D modeling study can be used to eliminate unfavorable engineering plans and to assist in selecting feasible engineering designs.

Results from the present study indicated that (1) flow and sediment transport are complex because of highly variable geometrical settings; (2) sufficient data collection, especially sediment data, is needed to select a favorable sediment-transport formula; (3) bank erosion occurs primarily at the outer banks of a meandering loop; and (4) modeling results can guide the design of bank protection structures with riprap or other engineering measures. However, these engineering recommendations were based on a 2-D modeling study when no additional field data are available that can be used to calibrate the model. The geometrical data were extracted from 1-ft contours. The inaccuracies of input data and assumptions in the 2-D model indicated that the results from the field case are qualitative rather than quantitative. These results are sufficient for engineers to prioritize restoration designs. However, details of hydrodynamic flow and sediment transport simulation require extensive model calibrations and verifications using more refined contour maps and more accurate flow and sediment data during flood events. Hydrodynamic-flow-field and sediment-transport data must to be collected to further calibrate and verify the simulated results.

## References

Arminini, A. and Di Silvio, G. (1988). “A one-dimensional model for the transport of a sediment mixture in on-equilibrium conditions.” J. of Hydraulic Research, 26(3), 275–292.Anwar, G. (1986). “Turbulent structure in a river bend.” Journal of Hydraulic Engineering, Vol. 112, No. 8, 657-669.

Crosato, A. (1990). “Simulation of meandering river processes.” Communications on hydraulic and geotechnical engineering, Technical report, Civil Engineering Department, Delft University of Technology.

Cui, Y., G. Parker, Lisle, T. E., Gott, J., Hansler-Ball, M. E., Pizzuto, J. E., Allmendinger, N. E., and Reed, J. M., 2003. Sediment Pulses in Mountain Rivers: 1. Experiments, *Water Recourses Research,* 39(9):ESG 3-1 to ESG 3-12.

Cui, Y., G. Parker, Pizzuto,J. and Lisle, T. E., 2003. Sediment Pulses in Mountain Rivers: 2. Comparison Between Experiments and Numerical Predictions, *Water Recourses Research*, 39(9):ESG 4-1 to ESG 4-11.

Cui, Y. and Parker, G., 2005. Numerical Model of Sediment Pulses and Sediment Supply Disturbances in Mountain Rivers. *Journal of Hydraulic Engineering*, 131(8):646-656.

Darby S. E., Alabyan A. M., and Van De Wiel M J. (2002). "Numerical simulation of bank erosion and channel migration in meandering rivers." Water Resources Research, AGU, Vol. 38, No. 9, 2-1-12.

Duan, J. G., Wang S. S. Y., and Jia Y. (2001), The application of the enhanced CCHE2D model to study the alluvial channel migration processes, J. of Hydraul. Res., 39(5), 469-480.

Duan J. G. (2004), Simulation of flow and mass dispersion in meandering channels, *J. of Hydraul. Eng.*, 130(10), 964-976.

Duan, J. G. (2005), Analytical approach to calculate rate of bank erosion, *J. of Hydraul. Eng.*, (131)11, 980-990.

Duan, J.G. and P.Y. Julien. (2005), Numerical simulation of the inception of meandering channel. *Journal of Earth Surface Processes and Land Forms* 30, 1093-1110.

Duan, J.G. and Nanda, S.K. (2006), Two-dimensional depth-averaged model simulation of suspended sediment concentration distribution in a groyne field, *Journal of Hydrology*, doi:10.1016/j.jhydrol.2205.11.055.

Einstein, H. A. (1950). “The bed-load function for sediment transportation in open channel flows.” U. S. Dept. Agric., Soil Conservation Service, T.B. no. 1026.

Engelund, F. and Skovgaard, O. (1973). “On the origin of meandering and braiding in alluvial streams.” Journal of Fluid Mechanics, Vol. 57, 289-302.

Engelund, F. and Fredsoe, J. (1982). “Hydraulic theory of alluvial river.” Advances in hydroscience, Vol. 13, Academic Press, New York, N. Y.

Hasegawa, K. (1981). “Bank-erosion discharge based on a non-equilibrium theory.” Proc. JSCE, 316, 37–50, Tokyo, Japan (in Japanese).

Hsieh, T. Y. and Yang, J. C. (2003). “Investigation on the suitability of two-dimensional depth-averaged models for bend-flow simulation.” J. Hydr. Eng. ASCE, Vol. 129, No. 8, 597-612.

Jia, Y. and Wang, S.Y. (1999). “Numerical model for channel flow and morphological change studies.” Journal of Hydraulic Engineering, Vol. 125, No.9, 924-933.

Lien, H.C., Hsieh, T.Y., Yang, J.C., and Yeh, K.C. (1999). “Bend flow simulation using 2D depth-averaged model.” Journal of Hydraulic Engineering, Vol. 125, No. 10, p1097-1108.

Meyer-Peter, R. and Müller, R. (1948), Formulas for Bedload Transport. *Proceedings 2nd Meeting International Association of Hydraulic Research*, Stockholm, Sweden, 39-64.

Molls, T., and Chaudhry, M. H. (1995). “Depth-averaged open–channel flow model.” J. Hydraul. Eng., 12(6), 453–465.

Odgaard, A. (1989a). “River meander model, I: Development.” Journal of Hydraulic Engineering, Vol. 115, No. 11, 1433-1450.

Odgaard, A. (1989b). “River meander model, II: Application.” Journal of Hydraulic Engineering, Vol. 115, No. 11, 1450-1464.

Parker, G., Klingeman, P. C., and McLean, D. L. (1982), Bedload and size distribution in paved gravel-bed streams. *J. Hydraulic. Division*, ASCE, Vol. 108, No. 4, 544–571

Parker, G. 1990. ‘‘Surface-based bedload transport relation for gravel rivers.’’ J. Hydraulic Research, Vol. 28, No. 4, 417–436.

Rahuel J. L., Holly, F. M., Chollet, J. P., Belleudy, P. J., and Yang, G. (1989). “Modeling of riverbed evolution for bedload sediment mixtures.” J. of Hydraul. Eng. ASCE, 115(11), 1521–1542.

van Rijn, L.C. (1984), Sediment transport, Part I: bed load transport, J. Hydraul. Eng., 110(10).

Shimizu, Y. and Itakura, T. (1989). “Calculation of bed variation in alluvial channels.” Journal of Hydraulic Engineering, Vol. 115, No. 3, 367-384.

Sutherland, D. G., M. Hansler-Ball, S. J. Hilton, and T. E. Lisle, 2002. Evolution of a Landslide-Induced Sediment Wave in the Navarro River, California, *Geological Society of America Bulletin*, 114(8):1036-1048.

Wu W., Rodi W., and Wenka T. (2000). “3D numerical modeling of low and sediment transport in open channels.” Journal of Hydraulic Engineering, Vol. 126, No.1, 4-5.

Wilcock, P. R. and Crowe, J. C. (2003), Surface-based transport model for mixed-size sediment. *J. Hydraul. Eng.* 129(2), 120-128.

Yang, C. T. (1984), Unit stream power and sediment transport, *J. of Hydraulic Engineering*, ASCE, Vol.110, No.12, 1783-1797.

Ye, J. and McCorquodale, J.A. (1997). “Depth-averaged hydrodynamic model in

curvilinear collocated grid." Journal of Hydraulic Engineering, Vol. 123, No.5, pp380-388.

Yeh, K. C. and Kennedy, J. (1993a). "Moment model of non-uniform channel bend flow I: Fixed beds." Journal of Hydraulic Engineering, Vol. 119, No. 7, 776-795.

Yeh, K. C. and Kennedy, J. (1993b). "Moment model of non-uniform channel bend flow, II: Erodible beds." Journal of Hydraulic Engineering, Vol. 119, No. 7, 796-815.

Yen, Chin-lien and Lee, Kwan Tun (1995). "Bed topography and sediment sorting in channel bend with unsteady flow." Journal of Hydraulic Engineering, Vol. 121, No.8, 591-599.

Table 1. Hydraulic parameters of experimental runs.

| Peak Flow Qp (m3/s) | Peak Flow Depth (m) | Duration of Rising Limb (min) | Duration of Hydrograph (min) |
|---|---|---|---|
| 0.0613 | 0.113 | 80 | 240 |

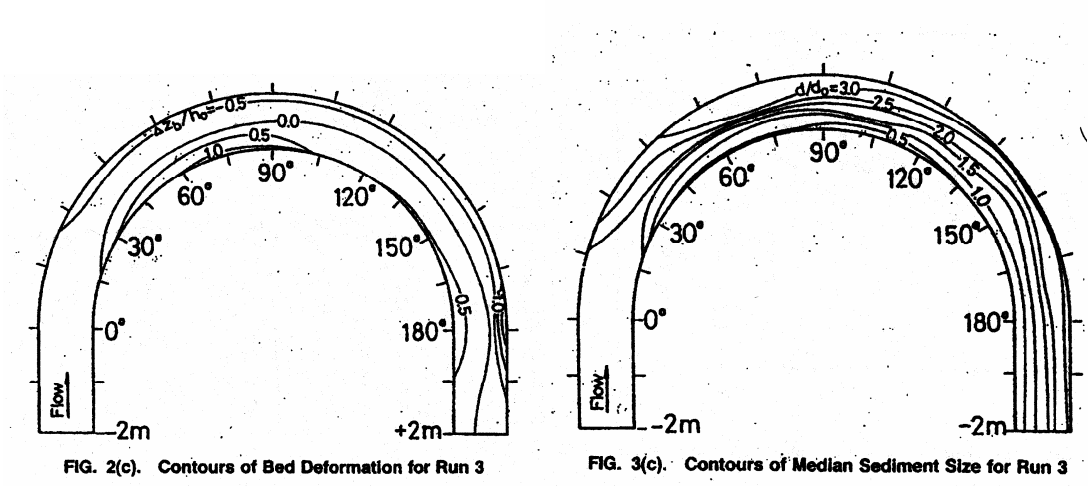


FIG. 2(c). Contours of Bed Deformation for Run 3

FIG. 3(c). Contours of Median Sediment Size for Run 3

Figure 1. Experimental measurements of bed-elevation changes and sediment-size distribution for run #3.

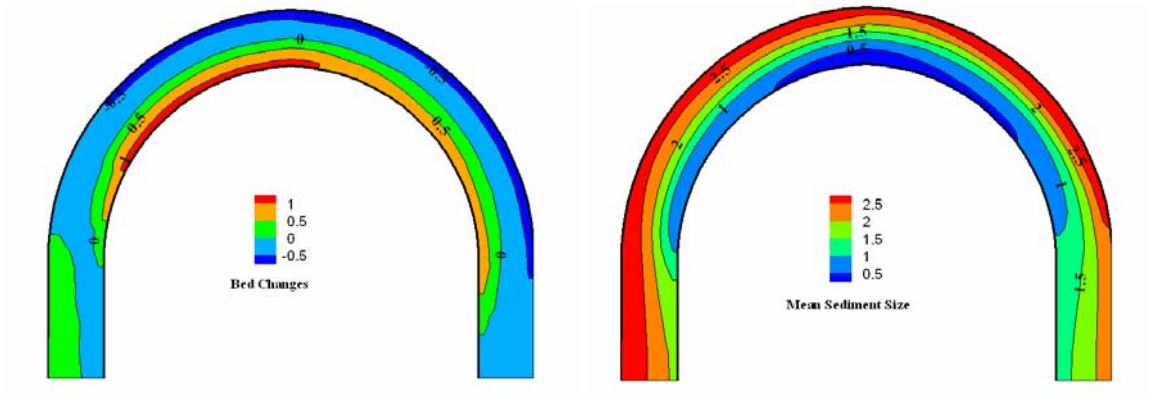


Figure 2. Simulated bed-elevation changes and sediment-size distribution for run #3.

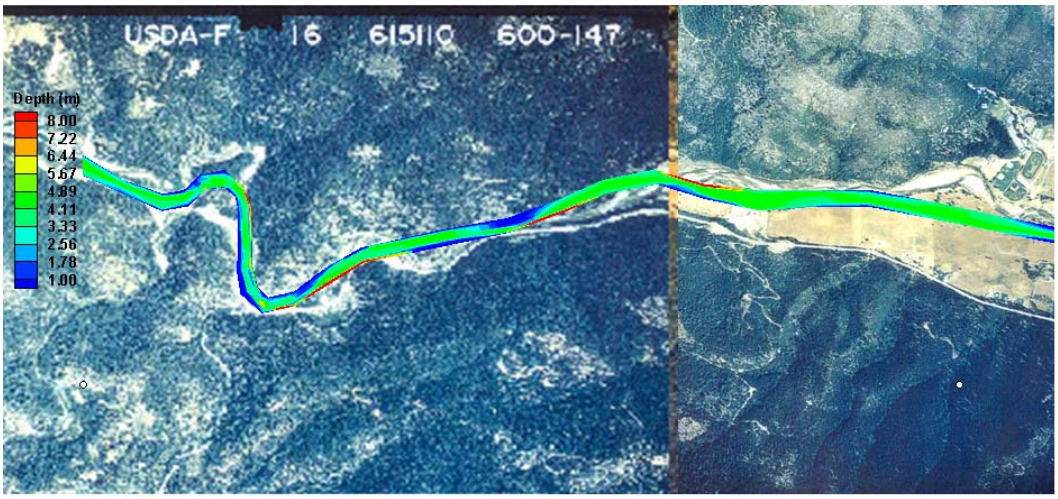


Figure 3a. Simulated flow depth after a bankfull discharge of seven days.

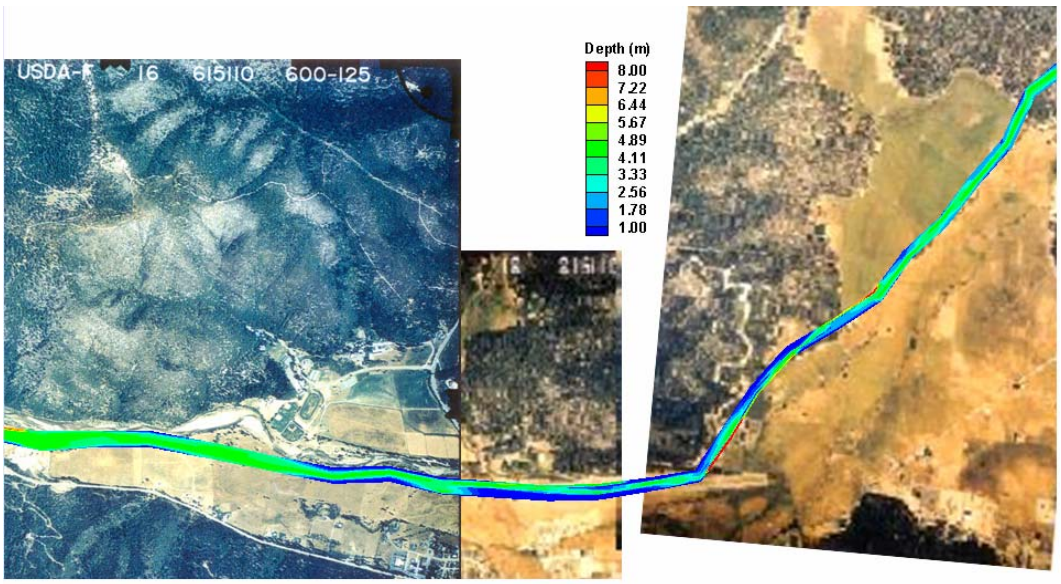


Figure 3b. Simulated flow depth after a bankfull discharge of seven days (continued).

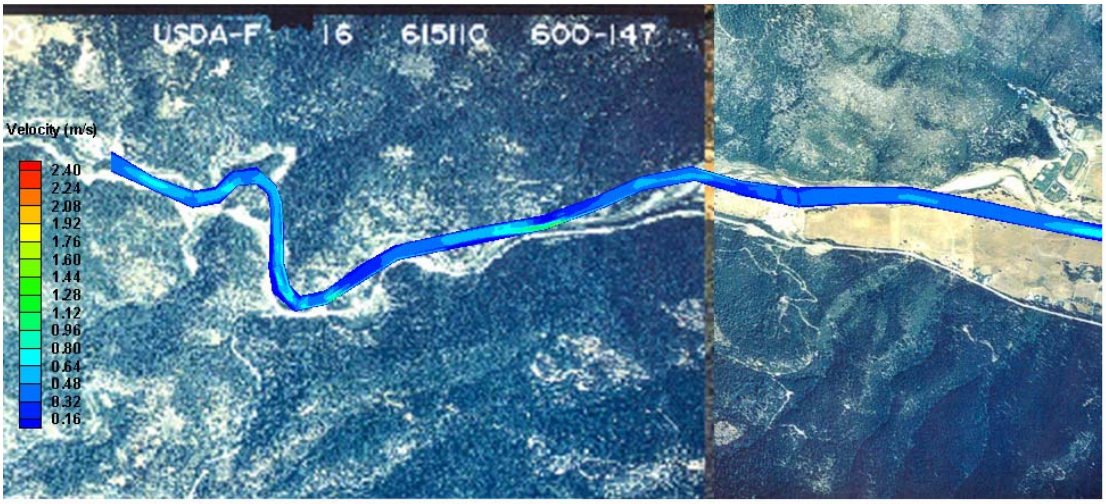


Figure 4a. Simulated flow velocity after a bankfull discharge of seven days.

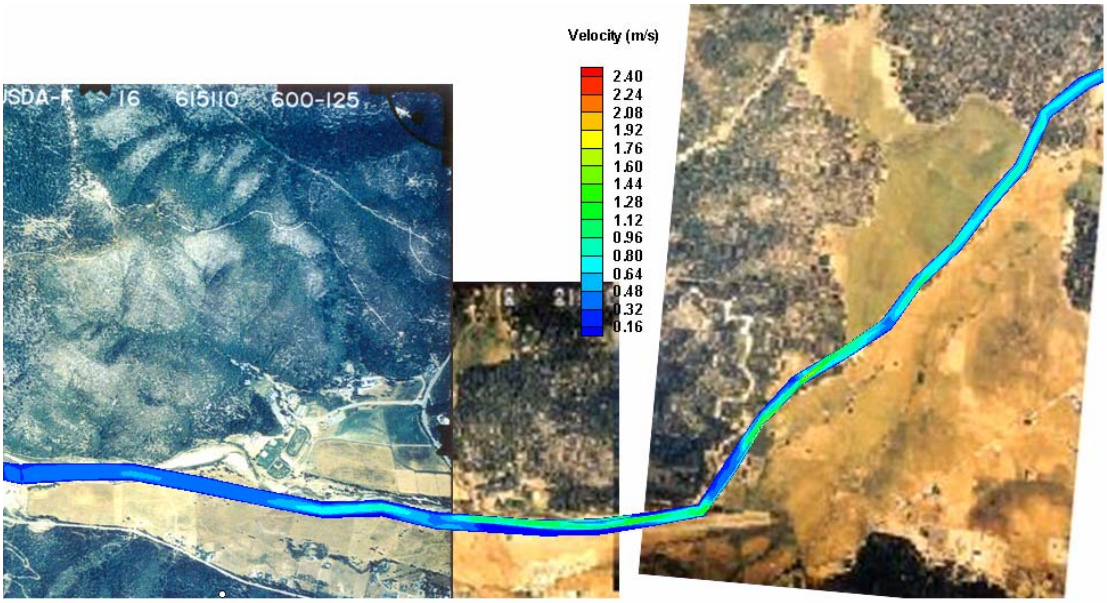


Figure 4b. Simulated flow velocity after a bankfull discharge of seven days (continued).

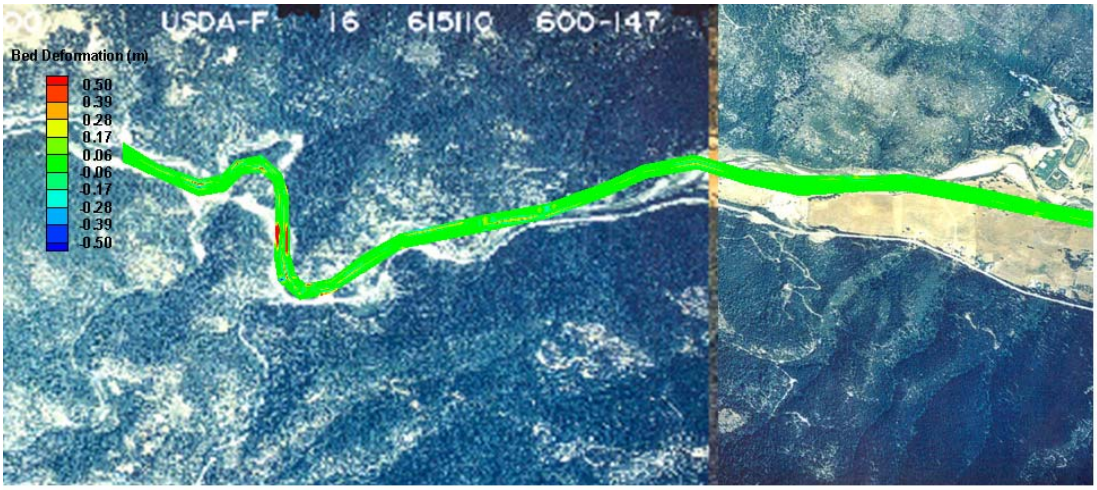


Figure 5a. Simulated bed-elevation change after a bankfull discharge of seven days.

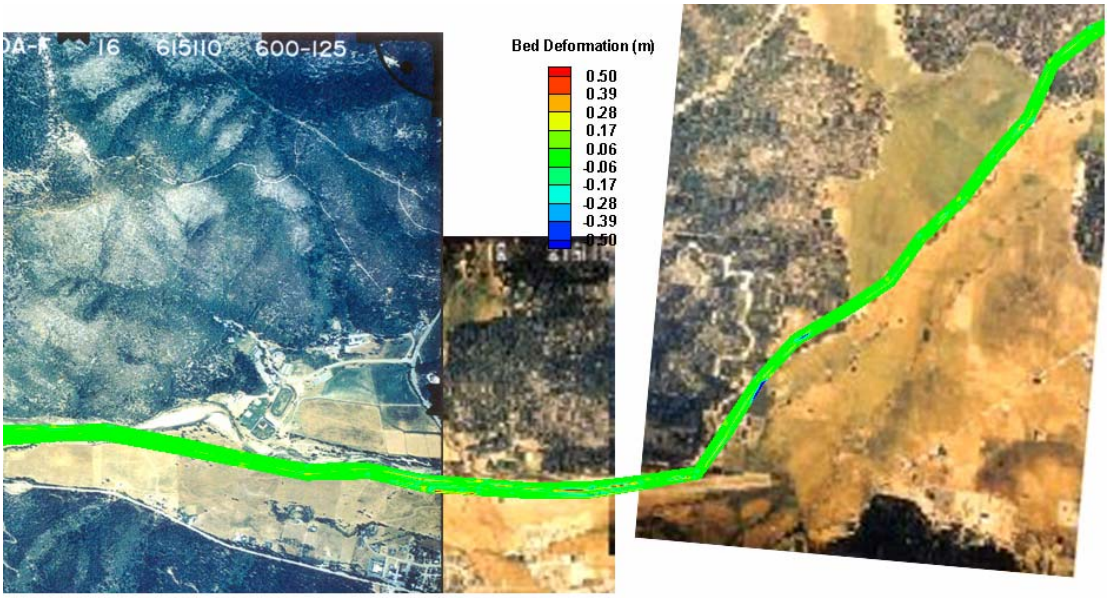


Figure 5b. Simulated bed-elevation change after a bankfull discharge of seven days (continued).

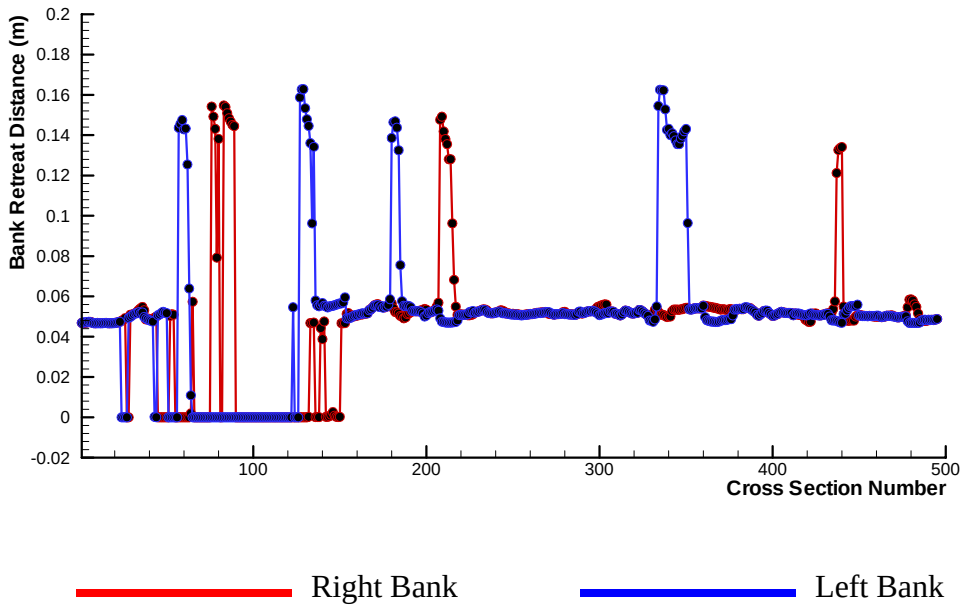


Figure 6. Distance of bank erosion after a seven-day bankfull flow.

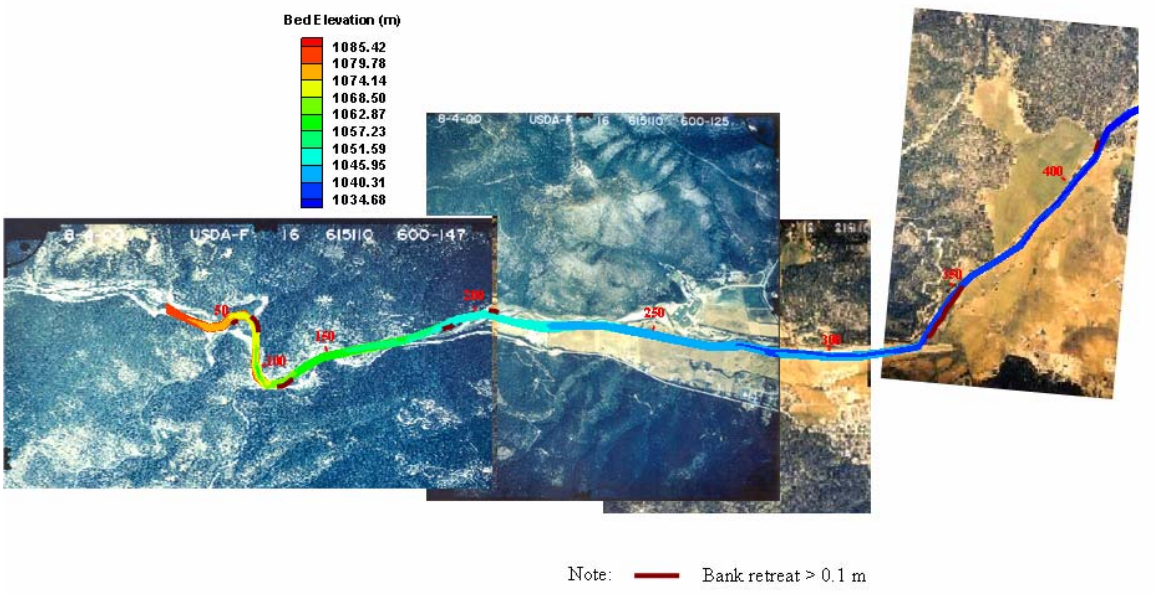


Figure 7. Reaches experiencing high rates of bank erosion after a seven-day bankfull event.